Magnetic dipole moments in single and coupled split-ring resonators

Yong Zeng,* Colm Dineen, and Jerome V. Moloney
Arizona Center for Mathematical Sciences, University of Arizona, Tucson, Arizona 85721, USA
(Received 21 October 2009; revised manuscript received 27 January 2010; published 22 February 2010)

We examine the role of magnetic dipoles in single and coupled pairs of metallic split-ring resonators by numerically computing their magnitude and examining their relative contributions to the scattering cross section. We demonstrate that magnetic dipoles can strongly influence the scattering cross section along particular directions. It is also found that the magnetic dipole parallel to the incident magnetic field may play a significant role in the linear response of coupled split-ring resonators.

DOI: 10.1103/PhysRevB.81.075116 PACS number(s): 42.70.−a

I. INTRODUCTION

In a seminal paper published in 1999, Pendry *et al.* proposed that an array of metallic split-ring resonators (SRRs) can, in the long-wavelength approximation, possess an effective negative permeability at its inductor-capacitor resonance.[1] This proposal lead to the development of an artificial structured medium, a metamaterial, consisting of interspaced SRR and metallic rods which simultaneously displays negative permeability and permittivity.[2] Such metamaterials are absent in nature and have potential application such as subwavelength or even perfect imaging.[3–6] Metallic SRR arrays are a popular building block for metamaterials and have attracted intensive attention in the last decade.[5,6] Such arrays are sometimes referred to as magnetic metamaterials due to the significant role played by magnetic dipoles in their optical response.

Experimentally single- and multilayered metallic single-slit SRR membranes have been fabricated and their optical responses are usually studied by measuring their transmission spectra at normal incidence.[7–10] A magnetic dipole moment perpendicular to the membrane, arising from a current circulating inside the SRR, is frequently mentioned as having a role in the observed transmission spectrum and in the coupling between adjacent SRRs.[9–16] However, we propose that the role of this magnetic dipole is unclear or even over emphasized in the literature perhaps due to the difficulty in experimentally measuring magnetic dipoles. Furthermore, rarely mentioned is the contribution from a magnetic dipole parallel to the incident magnetic field arising from the strongly localized conduction electrons near the metallic surfaces.[17]

The main aim of this article is to clarify the role of these magnetic dipoles by numerically computing their magnitude and examining their relative contributions to the scattering cross section. To achieve our purposes, we simulate the optical response of an isolated single SRR and a coupled pair of SRRs using the finite-difference time-domain (FDTD) method.[18,19] Our numerical results show that the strength of the magnetic dipoles can be determined by measuring the scattering cross section along particular directions. We also note that in certain circumstances the magnetic dipole parallel to the membrane plays a significant role. Finally, we numerically verify the qualitative assumption in earlier literature[9,10] that the magnetic dipole-dipole interaction must be considered to interpret the coupling strength between coupled SRRs.

The papers is arranged as follows. In Sec. II, we show that in the presence of an electric dipole the analytical expression for a magnetic dipole is not translational invariant. In Sec. III, we numerically compute the various electric and magnetic dipole moments and present a quantitative analysis of their relative contributions to the scattering cross section. The role of electric quadrupole in second-harmonic generation from an individual SRR are briefly discussed in an Appendix.

II. MULTIPOLE THEORY IN ELECTROMAGNETIC SCATTERING AND RADIATION

Let us first recall basic multipole theory in electromagnetic scattering and radiation.[17] For a localized current source $\mathbf{J}$, with sinusoidal time dependence, the relevant vector potential at position $\mathbf{r}$ is given by

$$\mathbf{A}(\mathbf{r}) = \frac{\mu_0}{4\pi}\int_v \mathbf{J}(\mathbf{r}')\frac{e^{ik|\mathbf{r}-\mathbf{r}'|}}{|\mathbf{r}-\mathbf{r}'|}d\mathbf{r}', \tag{1}$$

where $k=\omega/c$ is the wave number, and the integration is performed over the current source. Its asymptotic form

$$\lim_{r\to\infty}\mathbf{A}(\mathbf{r}) \approx \frac{\mu_0}{4\pi r}e^{ikr}\int_v \mathbf{J}(\mathbf{r}')e^{-ik\mathbf{n}\cdot\mathbf{r}'}d\mathbf{r}' \equiv \frac{\mu_0}{4\pi r}e^{ikr}\mathbf{p} \tag{2}$$

can be achieved by approximating $|\mathbf{r}-\mathbf{r}'|$ as r in the denominator while in the numerator $|\mathbf{r}-\mathbf{r}'|$ is replaced by $r-\mathbf{n}\cdot\mathbf{r}'$ with $\mathbf{n}=\mathbf{r}/r$ being the observation direction. Consequently, the far-zone electromagnetic fields can be formulated as

$$\mathbf{B}_s(\mathbf{r}) = \frac{ik\mu_0}{4\pi r}e^{ikr}\mathbf{n}\times\mathbf{p}, \quad \mathbf{E}_s(\mathbf{r}) = c\mathbf{B}_s\times\mathbf{n}. \tag{3}$$

We can now write the time-averaged power scattered per unit solid angle as[19]

$$\frac{dP_{\mathrm{sc}}}{d\Omega} = \frac{1}{2}\mathrm{Re}[r^2\mathbf{n}\cdot\mathbf{E}_s\times\mathbf{H}_s^*] = \frac{k^2\eta_0}{32\pi^2}|(\mathbf{n}\times\mathbf{p})\times\mathbf{n}|^2 \tag{4}$$

with $\eta_0=\sqrt{\mu_0/\epsilon_0}$ being the intrinsic impedance of free space. In addition, according to the optical theorem the extinction power P_{ex} taken from an incident wave $\mathbf{E}_0e^{i\mathbf{k}_0\cdot\mathbf{r}}$ takes the form[20]

$$P_{\mathrm{ex}} = \frac{1}{2}\mathrm{Re}\left[\mathbf{E}_0^* \cdot \int_v \mathbf{J}(\mathbf{r}')e^{-i\mathbf{k}_0\cdot\mathbf{r}'}d\mathbf{r}'\right] = \frac{1}{2}\mathrm{Re}[\mathbf{E}_0^* \cdot \mathbf{p}(\mathbf{k}_0)]. \tag{5}$$

This expression suggests that P_{ex} can be interpreted as interference between the incident wave and the forward scattering wave.[21]

The derivations above clearly demonstrate that the direction-dependent vector $\mathbf{p}$ contains all the information for scattering and/or radiation. Using Taylor expansion, we can reformulate $\mathbf{p}$ as

$$\mathbf{p} = \sum_n \frac{(-ik)^n}{n!}\int_v \mathbf{j}(\mathbf{r}')(\mathbf{n}\cdot\mathbf{r}')^n d\mathbf{r}'. \tag{6}$$

Mathematically, this transformation is always valid, however, to achieve physically meaningful quantities the spatial dimensions of the current volume must be much smaller than the incident wavelength. In other words, the quantity $k(\mathbf{n}\cdot\mathbf{r}')$ should be small compared to unity, and consequently the successive terms in the expansion fall off rapidly with n. The first term represents the electric dipole moment,

$$\mathbf{d} = \int_v \mathbf{j}(\mathbf{r}')d\mathbf{r}', \tag{7}$$

which corresponds to the electrostatic limit. The antisymmetric part of the second term is given by

$$ik\mathbf{n}\times\frac{1}{2}\int_v \mathbf{r}'\times\mathbf{j}(\mathbf{r}')d\mathbf{r}' \equiv ik\mathbf{n}\times\mathbf{m}, \tag{8}$$

with $\mathbf{m}$ standing for the magnetic dipole moment, while the symmetric counterpart $\int_v -ik/2[(\mathbf{n}\cdot\mathbf{j})\mathbf{r}'+(\mathbf{n}\cdot\mathbf{r}')\mathbf{j}]d\mathbf{r}'$ corresponds to the electric quadrupole.[17]

Despite the fact that these definitions can be found from any popular undergraduate electromagnetism textbook, determining the electric and magnetic dipole of a realistic system is not straightforward. The main reason is that as long as $\mathbf{d}$ exists $\mathbf{m}$ is not translational invariant (independent of the choice of origin of coordinates).[22] More specifically rewriting the above in a new coordinate system $\mathbf{x}$, which connects to the original as $\mathbf{x}=\mathbf{r}+\mathbf{a}$, we obtain an identical far-zone vector potential $\mathbf{A}$ but a slightly different $\mathbf{p}$ given by

$$\mathbf{p} = \int_v \mathbf{J}(\mathbf{r}')e^{-ik\mathbf{n}\cdot(\mathbf{r}'+\mathbf{a})}d\mathbf{r}'. \tag{9}$$

In this new coordinate system, the electric dipole $\mathbf{d}$ is identical to that defined in Eq. (7), however, the magnetic dipole $\mathbf{m}$ must be reformulated as

$$\mathbf{m} = \frac{1}{2}\int_v \mathbf{r}'\times\mathbf{J}(\mathbf{r}')d\mathbf{r}' + \frac{1}{2}\mathbf{a}\times\mathbf{d}. \tag{10}$$

The new formulation of the magnetic dipole $\mathbf{m}$ depends on $\mathbf{a}$ and is therefore not translationally invariant, similarly for the high-order multipoles.[23,24] In order to compare the relative contributions of the magnetic dipoles to the linear scattering we therefore take the advantage of the structural symmetries by choosing the *center of mass* as the coordinate origin.

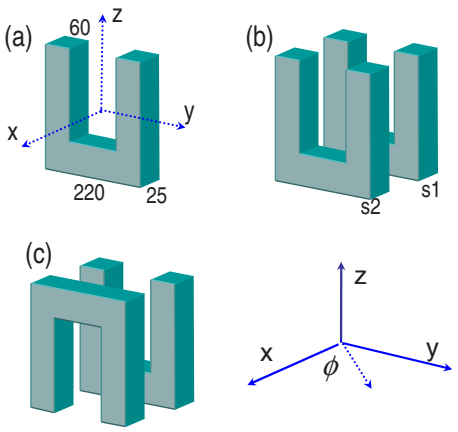

FIG. 1. (Color online) Schematic of (a) an individual split-ring resonator and two coupled split-ring resonators arranged in (b) Parallel configuration and (c) Opposite configuration. The separation between $s1$ and $s2$ is 30 nm. All other dimensions shown are in nanometers.

We apply this analysis to the configurations of gold SRRs embedded in vacuum as shown in Fig. 1. The structures are excited by a y-polarized plane wave propagating along the x direction. It excites not only a y-component electric dipole d_y, but also a magnetic dipole possessing both z and x components. The z component m_z is due to the strongly localized conduction electrons of the metal, while m_x is induced by the structural symmetry breaking. In order to simplify the following analysis we ignore higher-order multipoles and only consider contributions from the three dipoles d_y, m_x, and m_z.

From Eq. (4), the scattering cross section along the three primary axes are given by

$$\begin{aligned} &|d_y \mp ikm_z|^2, && \text{if } \mathbf{n} \text{ along the } \pm x \text{ direction;}\\ &k^2(|m_x|^2+|m_z|^2), && \text{if } \mathbf{n} \text{ along the } \pm y \text{ direction;}\\ &|d_y \pm ikm_x|^2, && \text{if } \mathbf{n} \text{ along the } \pm z \text{ direction.} \end{aligned} \tag{11}$$

For example, along the $\pm x$ direction the forward- or backward-scattering strength is influenced by the interference between the d_y and m_z dipoles, while the x-component magnetic dipole m_x does not contribute. This observation is at odds with the commonly stated assumption that the m_x dipole plays a significant role in one valley of the transmission spectrum of SRR arrays where it is often referred to as the magnetic resonance.[7] Similarly, along the y direction the scattering cross section is due solely to the m_x and m_z dipoles and receives no contribution from the electric dipole d_y. This observation may provide an insight on how to determine the relative magnitude of the various magnetic dipoles by experimentally measuring the scattering cross section along the orthogonal axes.

III. RESULTS AND DISCUSSIONS

To quantify the relative contributions of the various electric and magnetic dipole moments, we perform a numerical simulation of the structures shown in Fig. 1 using the FDTD method.[18,19] The relative dielectric constant of gold is fitted by the Drude model of

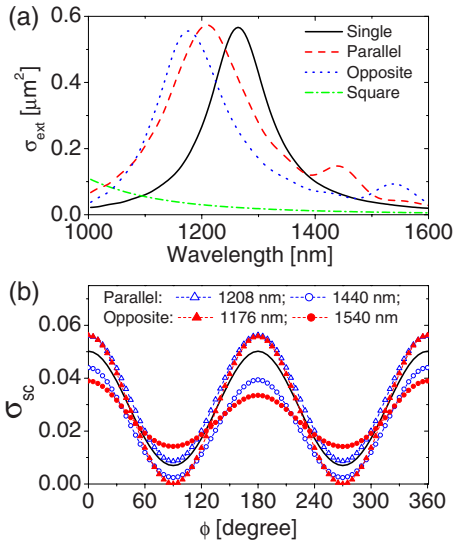

FIG. 2. (Color online) (a) Absolute extinction cross sections σ_{ext}. (b) Differential scattering cross section σ_{sc}, with dimensions of μm^2 per unit solid angle, as a function of the azimuthal angle ϕ. For the sake of clarity, the curves of 1440 nm wavelength and 1540 nm wavelength are amplified 10 times. The solid black curve corresponds to the individual split-ring resonator at 1264 nm wavelength. The incident plane wave propagates along the positive x [ϕ=0] direction and is y-polarized [ϕ=90].

$$\epsilon(\omega) = 1.0 - \frac{\omega_p^2}{\omega(\omega + i\gamma)}, \tag{12}$$

where $\omega_p = 1.367 \times 10^{16}$ s^{-1} is the bulk plasma frequency determined by the density of conduction electrons, $\gamma = 6.478 \times 10^{13}$ s^{-1} represents the phenomenological damping rate.[25] Using FDTD, with a center of mass coordinate system, we compute the polarization current inside the metallic structures and employ Eqs. (7) and (8) to determine the magnitude of the electric and magnetic dipole moments. Using Eqs. (4) and (5), which are independent of the chosen coordinate system, we compute the scattering and extinction cross sections.[19]

As before, the structures are excited with a plane wave propagating along the positive x direction and polarized in the y direction. The absolute extinction cross section σ_{ext} of the various SRR structures are shown in Fig. 2(a). For the single SRR (solid line), a peak corresponding to the fundamental plasmonic resonance was found at a wavelength of 1264 nm. A similar individual SRR is experimentally studied in Ref. 26 and the experimental extinction cross section and our numerical results are in excellent agreement. A periodic array of SRRs with lattice spacing of 305 nm was shown to have a fundamental resonance at 1212 nm wavelength, which is very close to the isolated SRR resonance indicating a weak coupling between adjacent SRRs.[27]

The scattering cross section σ_{sc} of the isolated SRR, at 1264 nm wavelength, as a function of the azimuthal angle ϕ in the xy plane is shown in Fig. 2(b) (solid line). This dependence curve can be fitted by $\cos^2\phi$ which suggests that the linear scattering of this individual SRR is dominated by a y-component electric dipole moment d_y. Based on the analysis related to Eq. (11), we can further estimate the magnitude of the magnetic dipoles from the scattering along the x and y directions. The plotted values of σ_{sc} along $\pm x$ directions [θ=0,180] are almost identical indicting a negligible z-component magnetic dipole m_z. Similarly for scattering along the $\pm y$ directions [θ=90,270] the cross section is nonzero indicating the presence of a finite total magnetic dipole. Consequently, we can deduce that the SRR possesses a considerable x-component magnetic dipole m_x.

To compare the relative strength of the numerically computed electric and magnetic dipole moments, we normalize them to the electric dipole moment d_s of the single SRR as follows:

$$\alpha = |d_y/d_s|, \quad \beta_x = k|m_x/d_s|, \quad \beta_z = k|m_z/d_s|, \tag{13}$$

and the results are shown in Table I. It is found that, for the individual SRR, β_x=0.25 while β_z is almost zero, in agreement with the scattering-cross-section-based analysis above. For comparison, we also plot in Fig. 2(a) the extinction cross section of a gold square of size 220×220 nm. In the wavelength range of 1000 to 1600 nm, the square exhibits no resonance peaks and has a weak extinction cross section consistent with its small normalized electric dipole of 0.23. However, it exhibits a larger z-component magnetic dipole m_z than the single SRR and, because of its symmetry, does not present a x-component magnetic dipole m_x.

We proceed to coupled SRRs oriented as depicted in Figs. 1(b) and 1(c) with a separation between $s1$ and $s2$ of 30 nm. Two different configurations are studied. The two SRRs are parallel to each other in the first arrangement (named Parallel) while in the second arrangement $s2$ is rotated 180° in the yz plane (named Opposite). Their extinction spectra are

TABLE I. Normalized magnitudes of electric and magnetic dipoles.

Structure	Wavelength (nm)	$\alpha[s_1,s_2]$	$\beta_x[s_1,s_2]$	$\beta_z[s_1,s_2]$	γ_m	γ_{eq}
Single	1264	1	0.25	<0.001		
Square	1264	0.23	0	0.001		
Parallel	1440	0.45 [1.65, −0.66]	0.08 [1.93, −0.93]	0.08 [0.68, 0.32]	0.08	0.004
Parallel	1208	1.02 [0.54, 0.46]	0.26 [0.56, 0.44]	0.01 [4.3, −3.3]	0.11	0.01
Opposite	1540	0.31 [2.06, −1.07]	0.18 [0.58, 0.42]	0.07 [0.63, 0.37]	0.36	0.025
Opposite	1176	0.99 [0.53, 0.47]	0.02 [9.1, −8.1]	0.008 [4.9, −3.9]	<0.001	<0.001

shown in Fig. 2(a). For both configurations, the 1264 nm peak of the individual SRR is split into two peaks induced by inter-SRR coupling. For the Parallel structure the peaks are located at 1208 and 1440 nm, and for the Opposite structure they are located at 1176 and 1540 nm. The larger separation between the peaks of the Opposite configuration indicates stronger inter-SRR coupling.[28] Furthermore, for each structure the shorter wavelength peak has a magnitude comparable to that of the individual SRR, while the longer wavelength peak has significantly reduced extinction cross sections.

For each configuration, the differential scattering cross section as a function of the angle ϕ in the xy plane is shown in Fig. 2(b). The scattering cross section along the y direction indicates the strength of the total magnetic dipole moment. Along the y direction $[\phi=90,270]$, the Parallel configuration at 1208 nm possesses a scattering cross section comparable to that of the single SRR. This is confirmed in Table I where β_x is 0.25 and 0.26 for the single SRR and Parallel configuration, respectively. For the Opposite configuration at 1176 nm, however, scattering along the y direction is almost zero indicating a negligible total magnetic dipole. This is also confirmed in the numerically computed values where β_z is 0.008 and β_x is an order of magnitude smaller than the single SRR with a value of 0.02.

The role of the z component of the magnetic dipole can be determined by looking at the difference in scattering between the positive and negative x directions. For example, the Opposite configuration at 1540 nm has a relative scattering difference of 14% along these two directions. This difference is induced by interference between a y-component electric dipole d_y and a z-component magnetic dipole m_z. Consequently, we can infer that this structure possesses a significant z-component magnetic dipole relative to the electric dipole. Again, this is confirmed in Table I where the ratio of magnetic to electric dipole strength β_z/α has a value of 0.23.

To distinguish the relative contribution from each SRR in the coupled structures, we compute their individual dipoles and normalize them to the total dipole moment. These values are listed in square brackets in Table I where values with opposite sign indicate the relevant dipoles are out of phase. For both Opposite and Parallel configurations, the y-component electric dipoles d_y are in phase at the shorter wavelength peaks and out of phase at longer wavelength peaks. This is consistent with the fact that a coupled system possesses a high-energy symmetric mode as well as a lower-energy antisymmetric mode. The inverse of this rule applies to the z-component magnetic dipoles m_z in that they are out of phase at shorter wavelengths and in phase at longer wavelengths due to the different symmetry of electric and magnetic fields. Because of the structural symmetry a more complicated phase relationship exists between the x-component magnetic dipoles m_x. For example, at the shorter-wavelength resonance they are in phase for the Parallel configuration while out of phase for the Opposite one. Table I further implies that although electric dipole-dipole interaction dominates the inter-SRR coupling, magnetic dipole-dipole interaction and in particular the m_x-m_x interaction must be included to interpret the fact that the Opposite configuration presents a larger separation between resonance peaks than its counterpart.

In the multipole expansion series, the electric quadrupole and the magnetic dipole are of the same order, it is therefore instructive to study the role of electric quadrupole in the linear scattering of the coupled structures. To measure their strength, the following normalized variables are defined:

$$\gamma_m = P_m/P_e, \quad \gamma_{eq} = P_{eq}/P_e, \tag{14}$$

where P_e is the total power radiated by the electric dipole, and P_m and P_{eq} is the total radiation exclusively coming from the magnetic dipole and the electric quadrupole, respectively. The numerical results are listed in Table I. For both configurations, γ_{eq} is approximately one order of magnitude weaker than γ_m, consequently the contribution of the electric quadrupole is much weaker than that of the magnetic dipole. Furthermore, the strongest electric quadrupole with $\gamma_{eq}=0.025$ is found from the Opposite configuration at 1540 nm. Therefore, we can safely neglect the electric quadrupole in the linear scattering process.

As suggested by the table, at the shorter wavelength peaks both coupled configurations possess an electric dipole comparable to that of the single SRR, however, their scattering along the transmission direction $[\theta=0]$ differ by 12%. The underlying reason is that the scattering cross section, as defined in Eq. (4), depends on the wavelength (so as the wave number k). Therefore, although the three structures have almost identical electric dipole, different exciting wavelength results in the 12% difference in their scattering along the transmission direction.

IV. CONCLUSIONS

This paper clarifies the role of magnetic dipoles in single and double metallic split-ring resonators by numerically computing their magnitudes and examining their relative contributions to the scattering cross section. We propose that the strength of the magnetic dipoles can be determined by measuring the scattering cross section along particular directions. It is demonstrated that the magnetic dipole parallel to the incident magnetic field plays a significant role for Opposite configuration at its longer wavelength resonance. By considering the relative phase between the partial dipoles possessed by individual SRRs in coupled configurations, we have shown that the electric dipole-dipole interaction dominates the coupling between adjacent SRRs and also that the magnetic dipole-dipole interaction is responsible for the larger resonance separation in the Opposite configuration.

ACKNOWLEDGMENTS

This work is supported by the Air Force Office of Scientific Research (AFOSR), under Grants No. FA9550-07-1-0010 and No. FA9550-04-1-0213. J.V.M. acknowledges support from the Alexander von Humboldt Foundation.

APPENDIX

Using a recently developed classical theory,[29] we numerically studied second-harmonic radiation from an individual SRR as schematically shown in Fig. 1(a). The fundamental

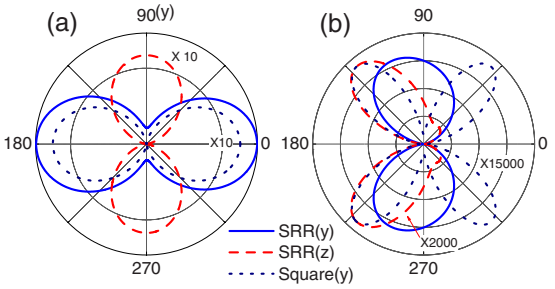

FIG. 3. (Color online) Linear (a) and second-harmonic (b) scattering of the individual split-ring resonator, specified in Fig. 1(a), in the yz plane. Both y-polarized (90°) and z-polarized (0°) incidences are considered. As a reference, a metallic square is also studied.

plane wave propagates along the positive x direction and has a wavelength of 1264 nm, corresponding to the fundamental resonances excited by a y-polarized light. Its linear scattering cross section in the yz plane is shown in Fig. 3(a). For comparison, we also considered a gold square of size 220 $\times$220 nm. Its linear response is quite close to that of the SRR with a z-polarized excitation, that is, they both possess an almost identical-strength electric dipole and a negligible magnetic dipole. The strongest electric dipole appears in the SRR with a y-polarized excitation.

Figure 3(b) plots second-harmonic radiation in the yz plane. The nonlinear radiation patters are significantly different with their linear scattering counterparts, which are induced by two reasons. The second-harmonic wavelength is 632 nm while the lateral size of the SRR is roughly 200 nm, higher-order multipoles are therefore expected to contribute considerably.[30] In addition, because of the selection rules of second-harmonic generation, the structural symmetry strongly influences the nonlinear process.[27,29] For example, the gold square has mirror symmetry along both z and y axes, its nonlinear radiation therefore presents a dominant electric quadrupole pattern. On the other hand, without the xy-plane mirror symmetry, the SRR allows the appearance of an electric dipole along the z direction.

Under the y-polarized incidence, the SRR possesses a significantly strong z-component electric dipole because of the excitation of the fundamental plasmonic resonance. We refer this electric dipole as D_z, and measure the strength of other multipoles in the following by normalizing them by D_z. Our simulations suggest that the SRR with the y-polarized excitation presents a weak magnetic dipole with a strength of merely 0.001. It, however, possesses a considerable electric quadrupole. The total radiation power from this quadrupole alone is about 5.9% of that coming from the electric dipole. On the other hand, the multipoles excited by the z-polarized incidence are quite different. We observe a feeble z-component electric dipole with a strength of 0.34 as well as a x-component electric dipole with a strength of 0.05. It is consistent with the results shown in Fig. 3(b) that the radiation strength of the y-polarized incidence is about 2000-fold stronger than the z-polarized incidence. It is further found that a negligible magnetic dipole (with a strength of 0.009) together with a considerable electric quadrupole in the SRR with z-polarized excitation. This quadrupole is very strong and its radiation power is 68.4% of that coming from the electric dipole. This result also consists with the fact that the radiation pattern of the SRR in the 90–270° regime is nearly identical to an electric-quadrupole pattern. Finally, we consider the gold square. Its nonlinear radiation is dominated by an electric quadrupole together with a weak x-component electric dipole. The radiation power from this dipole is 0.14 of that from the quadrupole. It is the coexistence of the electric dipole and quadrupole that results in the slightly distorted quadrupole pattern shown in Fig. 3(b).

*Present address: Department of Electrical Engineering, Pennsylvania State University, State College, Pennsylvania 16802, USA.

[1] J. B. Pendry, A. J. Holden, D. J. Robbins, and W. J. Stewart, IEEE Trans. Microwave Theory Tech. **47**, 2075 (1999).
[2] D. R. Smith, W. J. Padilla, D. C. Vier, S. C. Nemat-Nasser, and S. Schultz, Phys. Rev. Lett. **84**, 4184 (2000).
[3] J. B. Pendry, Phys. Rev. Lett. **85**, 3966 (2000).
[4] B. A. Munk, *Metamaterials: Critique and Alternatives* (Wiley, New York, 2009).
[5] R. Marqués, F. Martín, and M. Sorolla, *Metamaterials with Negative Parameters* (Wiley, New York, 2008).
[6] L. Solymar and E. Shamonina, *Waves in Metamaterials* (Oxford University, New York, 2009).
[7] S. Linden, C. Enkrich, M. Wegener, J. Zhou, T. Koschny, and C. M. Soukoulis, Science **306**, 1351 (2004).
[8] J. K. Gansel, M. Thiel, M. S. Rill, M. Decker, K. Bade, V. Saile, G. von Freymann, S. Linden, and M. Wegener, Science **325**, 1513 (2009).
[9] N. Liu, H. Liu, S. Zhu, and H. Giessen, Nat. Photonics **3**, 157 (2009).
[10] I. Sersic, M. Frimmer, E. Verhagen, and A. F. Koenderink, Phys. Rev. Lett. **103**, 213902 (2009).
[11] N. Liu, S. Kaiser, and H. Giessen, Adv. Mater. **20**, 4521 (2008).
[12] A. Schneider, A. Shuvaev, S. Engelbrecht, S. O. Demokritov, and A. Pimenov, Phys. Rev. Lett. **103**, 103907 (2009).
[13] F. Hesmer, E. Tatartschuk, O. Zhuromskyy, A. A. Radkovskaya, M. Shamonin, T. Hao, C. J. Stevens, G. Faulkner, D. J. Edwards, and E. Shamonina, Phys. Status Solidi B **244**, 1170 (2007).
[14] T. Q. Li, H. Liu, T. Li, S. M. Wang, J. X. Cao, Z. H. Zhu, Z. G. Dong, S. N. Zhu, and X. Zhang, Phys. Rev. B **80**, 115113 (2009).
[15] X. Xiong, W.-H. Sun, Y.-J. Bao, R.-W. Peng, M. Wang, C. Sun, X. Lu, J. Shao, Z.-F. Li, and N.-B. Ming, Phys. Rev. B **80**, 201105(R) (2009).
[16] M. Decker, S. Burger, S. Linden, and M. Wegener, Phys. Rev. B **80**, 193102 (2009).
[17] J. D. Jackson, *Classical Electrodynamics*, 3rd ed. (Wiley, New York, 1999).
[18] A. Taflove and S. C. Hagness, *Computational Electrodynamics: The Finite-Difference Time-Domain Method*, 2nd ed. (Artech House, Boston, 2000).
[19] Y. Zeng and J. V. Moloney, Opt. Lett. **34**, 1600 (2009).

[20] P. Yang and K. N. Liou, J. Opt. Soc. Am. A Opt. Image Sci. Vis **13**, 2072 (1996).
[21] M. I. Mishchenko, J. Quant. Spectrosc. Radiat. Transf. **70**, 811 (2001).
[22] R. Merlin, Proc. Natl. Acad. Sci. U.S.A. **106**, 1693 (2009).
[23] R. E. Raab and O. L. De Lange, *Multipole Theory in Electromagnetism* (Oxford University, New York, 2005).
[24] N. Papasimakis, V. A. Fedotov, K. Marinov, and N. I. Zheludev, Phys. Rev. Lett. **103**, 093901 (2009).
[25] *Handbook of Optical Constants of Solids*, edited by E. D. Palik (Academic, New York, 1985).
[26] M. Husnik, M. W. Klein, N. Feth, M. König, J. Niegemann, K. Busch, S. Linden, and M. Wegener, Nat. Photonics **2**, 614 (2008).
[27] Y. Zeng and J. V. Moloney, Opt. Lett. **34**, 2844 (2009).
[28] J. J. Sakurai, *Modern Quantum Mechanics*, Revised ed. (Addison-Wesley, Reading, MA, 1994).
[29] Y. Zeng, W. Hoyer, J. Liu, S. W. Koch, and J. V. Moloney, Phys. Rev. B **79**, 235109 (2009).
[30] J. Petschulat, A. Chipouline, A. Tünnermann, T. Pertsch, C. Menzel, C. Rockstuhl, and F. Lederer, Phys. Rev. A **80**, 063828 (2009).